

# A Physically Based Approach to the Accurate Simulation of Stiff Fibers and Stiff Fiber Meshes

Dominik L. Michels, J. Paul T. Mueller, Gerrit A. Sobottka

*michels@cs.stanford.edu*

*Computer Science Department, Stanford University, 353 Serra Mall, Stanford, US-CA 94305*

---

## Abstract

We devise a physically based approach to the accurate simulation of stiff fibers like human hair, wool, or yarn. For that we describe fibers as three-dimensional coupled oscillator networks. The application of special analytical mapping expressions allows us to mimic the existence of Young's and shear modulus in the oscillator network so that real material parameters can be used. For the efficient numerical treatment of the stiff equations of motion of the system a *Damped Exponential Time Integrator (DETI)* is introduced. This type of integrator is able to take large time steps during the solution process of the stiff system while sustaining stability. It also handles Rayleigh damping analytically by employing the closed-form solution of the fully damped harmonic oscillator. We validate the fiber model against the outcome obtained by solving the special Cosserat theory of rods. Moreover, we demonstrate the efficiency of our approach on some complex fiber assemblies like human hair and fiber meshes. Compared to established methods we reach a significant speed up and at the same time achieve highly accurate results.

*Keywords:* Cosserat Rods, Exponential Integrators, Fibers and Fiber Meshes, Hair Simulation.

---

## 1. Introduction

Fibers are slender structures with a negligible small diameter compared to their length. Typical examples for such structures comprise human hair, spaghetti, ropes, hoses, undersea cables, or woven textiles. The numerical simulation of fibers—especially human hair—has gained increased attention in scientific and visual computing over the past years. The first models proposed by the community are based on simple mass-spring systems and are therefore unable to capture naturally occurring deformation modes like bending and twisting of a fiber. Recent models rely upon continuum mechanical rod theories such as the one proposed by Kirchhoff in his original work [23]. The notion of bending and twisting is an integral part of the Kirchhoff rod theory. Combined with the concept

of constitutive relations that allows for the application of real mechanical parameters it makes high demands on the numerical solution process as bending, twisting, and elongation of natural fibers evolve on time scales that differ by orders of magnitude. This phenomenon is commonly referred to as “stiffness of the system.” The stiffness of the underlying system enforces slowness of common discretization methods and as such prohibits the simulation of a larger number of fibers in an assembly in passable time. So-called exponential integrators on the other hand can deal with such stiff systems remarkably well as we shall demonstrate in this contribution. In combination with carefully constructed networks of damped harmonic oscillators, this allows us to simulate large assemblies of fibers or fiber meshes with authentic

mechanical parameters in real-time without resorting to numerically more involved rod theories. At the heart of our approach lies a *Damped Exponential Time Integrator (DETI)* that utilizes the analytic solution of the damped harmonic oscillator. Besides the efficient treatment of stiffness, this enables one to treat damping in a purely analytic fashion and thus allows for gauging the system’s internal viscosity according to measured data.

## 2. Related Work

The problem of the numerical simulation of fibers, especially human hair, dates back at least to [32] where a simple mass-spring model is used to simulate single hair fibers of a non-interacting assembly. The authors of [1] employed the cantilever beam equation, a fourth order ODE from the field of mechanical engineering in order to model up to 20 000 single hair fibers on a human head. In [27] the classical reduced coordinate formulation of a multibody chain with joints between the links, which was formerly used in the field of robotics to calculate the forward dynamics of industrial manipulators, has been introduced to the visual computing community. The main advantage of this approach lies in the fact that the bending and twisting angle between consecutive links can be measured easily by means of local triads that are attached to the rigid links and evolve forward in time and space as the forward dynamics of the manipulator is calculated. For a small number of links, this is efficiently done with the algorithm of Featherstone, that solves for the joint forces in a two-pass process, cf. [17] or the work of [27] for a beautiful and comprehensible derivation of Featherstone’s algorithm. The notion of multibody chains with joint constraints has been adopted for the purpose of hair simulation by [14, 21]. While the former work utilizes the multibody chain to model individual fibers of a hairstyle, in [14] it is used to simulate the center line of a hair wisp. In contrast to the conventional approach with hard joint constraints used in [27], the authors of [14] replaced the joints by bending and shear springs. This leads to soft constraints allowing one to overcome the hard constraint forces at the joints.

From a continuum mechanics point of view, the mechanical behavior of a flexible slender structure or elastic rod that is subject to external uniform loads, e.g. gravity, is described by the classical theory of the Kirchhoff rod, cf. [23]. The equilibrium shape of the rod is governed by a set of non-linear and coupled partial differential equations. Each infinitesimal thin material cross section plane of the rod is furnished with a orthonormal triad that allows one to measure different types of local deformations like bending and twisting. The theory of the Kirchhoff rod is an intrinsically constrained model insofar as the cross section plane is not allowed to undergo shear or dilation motion, so that the rod described therein is unshearable and inextensible. Neglecting these two deformations is not uncommon as their effect usually takes place on a much smaller scale than bending and twisting deformations.

The static Kirchhoff equations have first been employed in [31] to simulate strands of surgical suture. In the non-static case the Kirchhoff rod has been adopted for the simulation of hair fibers by [9, 37]. In [9] the equations of motion of the rod are recaptured by using the Lagrange formalism on the energy function that solely depends on the curvature function of the rods centerline, which is assumed to be constant along the helical elements of the discretized rod. The spatial discretization is solved exactly, while the resulting ODE is solved numerically in time using a semi-implicit Euler scheme. After small modifications, Featherstone’s algorithm for linked multibody chains also applies to the model of [9], cf. [8]. This results in a reduced coordinate formulation. In [37] on the other hand the classical Kirchhoff equations are discretized by means of an unconditionally stable, Newmark-like integration scheme to solve the underlying two-point boundary value problem.

In a certain sense the classical reduced coordinate formulation of the multibody chain can be considered as a special case of the discretized Kirchhoff rod. Instead of discretizing the underlying equation system directly some authors prefer to derive discrete rod models, in which the discrete equations of motion follow from the application of the Lagrangian principle to the discrete energy expressions derived for the individual segments of the rod, cf. [7, 38] and

the aforementioned work of [9]. The main difference is the way how the energy is expressed. Classically, this is done by measuring the deviation of the current from some initial reference configuration of the rod. In [7] the reference configuration is determined by the so-called Bishop frame. It describes the most relaxed or twist-free configuration of the rod as opposed to the more prominent Frenet frame. The authors of [40] propose a position based method for elastic rod simulation that heavily borrows from prior work [7, 38]. Specifically, they introduce so-called ghost points along edges in order to furnish them with a material frame. According to the authors interactive rates are achieved for 200 fibers consisting of 20 segments each. The problem of dense equations systems that typically appear in maximum coordinate formulations has been addressed to a certain degree by the authors of [6] by using for elastic rods time-parallel transport of reference frames. This leads to a Hessian matrix with banded structure that promotes faster dynamics computations up to one order of magnitude.

While Kirchhoff rods are relatively new to the field of visual computing, the adaption of coupled oscillator networks, commonly called mass-spring systems, is well-established and much easier to handle in terms of the numerical effort that has to be made in order to simulate fibers. One of the major shortcomings is that the consideration of twisting and bending deformations is only possible in a rather ad-hoc fashion. In [13] a mass-spring model was proposed in order to approximate the deformation of a hair wisp during collisions. The underlying three-dimensional scaffold of connected particles already allowed to capture moderate bending and twisting deformations. The first model that accounts for twisting deformation without using a scaffold around the fiber was proposed in [36] where the dynamics of a thinned out hair style with 10 000 single fibers have been simulated. A single fiber is constructed using a particle system that is furnished with additional ad-hoc springs to account for fiber twisting (“altitude springs”). Numerical integration is performed using a modified central Newmark scheme adopted from prior work of [12].

In this regard our specific contributions are as follows: we devise a physically based approach to the ac-

curate simulation of stiff fibers and fiber meshes. For that, fibers are described as three-dimensional coupled oscillator networks because these are much easier to handle in complex contact situations than more strict continuum formulations like Cosserat rods, cf. [2]. Also, we use special analytical expressions in order to adapt the mapping of real values of the Young’s and the shear modulus to the oscillator network and their spring constants, respectively. To evolve forward in time the stiff equations of motion of the fibers a *Damped Exponential Time Integrator* (DETI) is devised that is able to handle the stiff components of the equations of motion as well as Rayleigh damping fully analytically by employing the closed-form solution of the damped harmonic oscillator. This is accompanied by a thorough validation of the single fiber model against the Cosserat rod equations. Finally, we present convincing numerical examples as proof of concept including comparisons to state-of-the-art approaches.

### 3. A Numerical Model for Stiff Fibers

It is well known that in some natural as well as artificial fibers the resistance exhibited against longitudinal expansion is commonly much larger than that against bending or shearing. On the other hand, there are also a few long and thin systems which stretch easily while resisting bending. The stiffness ratio makes the governing equations inherently stiff as the underlying processes evolve on time scales that differ by orders of magnitude. This enforces small step sizes with common integrators. The stiff behavior of fibers has lead to the development of a series of models that either neglect the longitudinal dilation by enforcing strict non-extendibility through the introduction of appropriate constraints (cf. e.g. [7, 38]). Other approaches try to get the problem under control with strain limiting (i.e. avoiding the extent using hard constraints) post-processing steps, cf. e.g. [36], or rely on reduced coordinate formulations (cf. [9, 20, 27]) that normally lead to dense equation systems. For small numbers of links the forward dynamics of a serial multi body chain can be computed in linear time with the algorithm of Featherstone, cf. [17].

However, in our approach we resort to classic mass-spring systems as their flexibility gives us the freedom to handle large systems with collisions very efficiently although the focus of this contribution is not collision handling in fiber assemblies. Besides, typical attributes of mass-spring systems have been addressed in several publications, e.g. dependency on topology and resolution, cf. [16]; parameter estimation, cf. [10]; anisotropic material behavior, cf. [39]; non-linear material properties, cf. [15].

### 3.1. Cuboidal Oscillator Networks with Parameter Mapping

Each single fiber consists of coupled oscillators that are connected in such a way that the fiber axis is enveloped by a chain of cuboidal elements. Each cuboid is composed of twelve tension springs, that are placed along its edges and four inner diagonal springs for preventing a volumetric collapse during the simulation, cf. Fig. 1. This follows directly from the application of Occam’s razor: the building blocks must be at least cuboids as prismetoids cannot withstand volumetric collapse even with diagonal springs on the side faces. In addition, it has been pointed out in [4] that the diagonal springs fully determine the shear modulus. The cuboidal model can handle deformational modes like bending, twisting, and stretching. The strain is limited by assigning to the tensile springs a very high stiffness value. One of the major arguments against the application of systems of coupled oscillators has often been that it is hard or even impossible to map real mechanical parameters like the Young’s or the shear modulus to the system. Consequently, this problem has already been approached by other research groups. One of the first studies of such mappings for two-dimensional triangle meshes (membranes) was presented in [41]. As the expressions derived by the author have been found to be inexact, an extension to the three-dimensional case was proposed by the authors of [4, 5] and similarly in [35]. In [25] the authors derive analytic expression by comparing coefficients from a finite element formulation. A general finite element mapping procedure for defining oscillator network representations of solids was published by [19]. The derivation of expressions that allow us to map the Young’s and

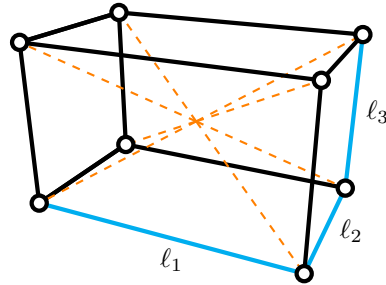


Figure 1: Cuboidal element enclosing the center line of the fiber. The edges as well as the diagonals act as springs with certain stiffnesses. This particular connectivity allows one to map the Young’s and the shear modulus to a cuboidal element.

the shear modulus to the spring constants of the oscillator network of a fiber is given in Appendix A.

### 3.2. Equations of Motion

The system state of the fiber can be described by the displacement function  $\mathbf{x} : \mathbb{R}^{\geq 0} \rightarrow \mathbb{R}^{3N}$  fulfilling the equations of motion, which returns the  $N$  Cartesian displacements for a given point  $t$  in time and can be derived from the autonomous standard Lagrangian function which we omit here for brevity. The second order equations of motion read

$$\mathbf{M}\ddot{\mathbf{x}}(t) + \mathbf{D}\dot{\mathbf{x}}(t) + \mathbf{K}\mathbf{x}(t) + \mathbf{\Lambda}(\mathbf{x}(t)) = \mathbf{0},$$

where  $\mathbf{x}(t) \in \mathbb{R}^{3N}$  denotes the current displacements from the initial positions of the particles,  $\mathbf{M} \in \mathbb{R}^{3N \times 3N}$  is the diagonal mass matrix, and  $\mathbf{K} \in \mathbb{R}^{3N \times 3N}$  the stiffness matrix. The nonlinearity  $\mathbf{\Lambda}(\mathbf{x}(t)) \in \mathbb{R}^{3N}$  collects other nonlinear (external) forces.

System dissipation due to internal friction and similar forces that result in a decrease of energy are formulated with an appropriate damping matrix

$$\mathbf{D} := \mathbf{M} \sum_{i=0}^l \alpha_i (\mathbf{M}^{-1} \mathbf{K})^i$$

with model parameters  $\alpha_0, \dots, \alpha_l$ . For  $l = 1$  one gets the (linear) Rayleigh model, cf. [24].

As already mentioned the numerical treatment of this differential equation system is delicate because

the dynamics of the system evolves on time scales of different sizes. This is where the *Damped Exponential Time Integrator* comes into play.

### 3.3. A Damped Exponential Time Integrator (DETI)

As the deformation modes are essential parts of the fiber model introduced above the system is inherently stiff. We approach the numerical treatment of the stiff equations by devising a *Damped Exponential Time Integrator* (DETI). The DETI belongs to a class of numerical integration schemes that are able to handle systems with arbitrary stiffness ratios effortlessly. Another big advantage of the DETI is its analytic treatment of system damping: it allows one to switch from arbitrary underdamping to critical damping (the state where the kinetic energy of the system approaches zero without oscillating), including overdamping without causing any numerical instability.

With this tool at hand there is no further need to elude the stiffness problem by introducing workarounds, for example implicit linear springs with a subsequent strain limiting approach like it was proposed in [36] because the DETI tackles the stiffness problem at its root.

In order to guarantee an efficient and stable solution process of the stiff equations of motion, in [26] the authors studied an *Exponential Time Integrators* (ETI), that are closely related but not identical to the integrator derived in this section. In order to handle the stiff components without numerical instabilities, the ETI utilizes the analytic solution of the linear part of the equations of motion. This leads to the accurate preservation of the underlying structure of the equations of motion. Unfortunately, damping is handled purely numerically which violates structure preservation leading to the need of significantly larger temporal step sizes and therefore to a poor efficiency when simulating complex fiber assemblies. In contrast to the undamped ETI approach proposed in [26], we overcome this shortcoming by exploiting the fact that the *damped* harmonic oscillator also has a closed-form solution. This allows us to avoid a separate numerical treatment of the damping part of the equations of motion. Therefore, we start with the an-

alytic solution of the homogeneous part of the equations of motion with  $\mathbf{\Lambda} = \mathbf{0}$  given by

$$\mathbf{x}(t) = \exp\left(-t\hat{\mathbf{D}}\right) \cos\left(t\hat{\mathbf{K}}\right) \mathbf{x}_0$$

with  $\hat{\mathbf{D}} := \frac{1}{2}\mathbf{M}^{-1}\mathbf{D}$ ,  $\hat{\mathbf{K}} := \sqrt{\mathbf{M}^{-1}\mathbf{K} - \hat{\mathbf{D}}^2}$ , and  $\mathbf{x}_k := \mathbf{x}(k\Delta t)$  for all  $k \in \mathbb{N}_0$ . This expression holds for the case of linear Rayleigh damping and a uniform mass distribution, i.e.  $\mathbf{M} = m\mathbf{1}$  with constant particle mass  $m$ , which we assume in the following. From this we derive a two step method to compute  $\mathbf{x}_{k+1}$  from  $\mathbf{x}_k$  and  $\mathbf{x}_{k-1}$  by the application of Chebyshev polynomials and obtain

$$\mathbf{x}_{k+1} = \exp\left(-\left(k+1\right)\Delta t\hat{\mathbf{D}}\right) \mathbb{T}_{k+1}\left(\cos\left(\Delta t\hat{\mathbf{K}}\right)\right) \mathbf{x}_0.$$

In this context,  $\mathbb{T}_k$  denotes the first kind Chebyshev polynomial of order  $k$  defined recursively by the relation

$$\mathbb{T}_{k+1}(\mathbf{A}) := \begin{cases} 2\mathbf{A}\mathbb{T}_k(\mathbf{A}) - \mathbb{T}_{k-1}(\mathbf{A}), & \text{if } k \in \mathbb{N}^{\geq 2} \\ \mathbf{A}, & \text{if } k = 1 \\ \mathbf{1}, & \text{if } k = 0 \end{cases}$$

generalized to square matrix arguments, which corresponds to  $\mathbb{T}_k = \cos(k \arccos(\mathbf{A}))$ . This can easily be proved with the use of the relation

$$\cos(\mathbf{A}) \cos(\mathbf{B}) = \frac{1}{2} (\cos(\mathbf{A} - \mathbf{B}) + \cos(\mathbf{A} + \mathbf{B}))$$

for general square matrices  $\mathbf{A}$  and  $\mathbf{B}$ . We evaluate the solution of the homogeneous system and end up with

$$\begin{aligned} \mathbf{x}_{k+1} &= 2 \exp\left(-\Delta t\hat{\mathbf{D}}\right) \cos\left(\Delta t\hat{\mathbf{K}}\right) \mathbf{x}_k \\ &\quad - \exp\left(-2\Delta t\hat{\mathbf{D}}\right) \mathbf{x}_{k-1}. \end{aligned}$$

In order to handle the inhomogeneous equation we add to this analytic solution of the homogeneous part a numerical solution of the inhomogeneity. Integrating  $\mathbf{\Lambda}$  twice explicitly leads to the scheme

$$\begin{aligned} \mathbf{x}_{k+1} &= 2 \exp\left(-\Delta t\hat{\mathbf{D}}\right) \cos\left(\Delta t\hat{\mathbf{K}}\right) \mathbf{x}_k \\ &\quad - \exp\left(-2\Delta t\hat{\mathbf{D}}\right) \mathbf{x}_{k-1} \\ &\quad - \Delta t^2 \mathbf{M}^{-1} \text{sinc}^2\left(\Delta t\hat{\mathbf{K}}\right) \mathbf{\Lambda}_k^\bullet \end{aligned}$$

with

$$\Lambda_k^\bullet = \Lambda \left( \text{sinc} \left( \Delta t \hat{K} \right) \mathbf{x}_k \right).$$

Since high external frequencies tend to produce numerical instabilities, we have added a low-pass sinc filter in both integration steps and filter the argument of the inhomogeneity in a similar way. This choice corresponds to a symplectic integration scheme for  $\mathbf{D} = \mathbf{0}$ .

The price to pay for a semi-analytical treatment of stiff linear forces is the need to evaluate functions  $f(\cdot)$ , such as  $\exp(\cdot)$ ,  $\cos(\cdot)$ , and  $\text{sinc}^2(\cdot)$  for scaled matrix arguments  $\mathbf{A} \in \{\tau \hat{K}, \tau \hat{D} | \tau \in \mathbb{R}\}$ . This is a non trivial computational task, that we address using a Krylov-based reduction [33] for efficiency.<sup>1</sup>

*Krylov Subspace Projection.* The key idea is to prevent the direct computation of the matrix functions, and instead, calculate the action of the matrix  $f(\mathbf{A})$  on a vector  $\mathbf{x} \in \mathbb{C}^{3N}$ . A simple approach to approximate  $f(\mathbf{A})\mathbf{x}$  is to use the truncated Taylor series of  $f$  of degree  $m - 1$  that is given by  $\sum_{k=0}^{m-1} a_k \mathbf{A}^k \mathbf{x}$ . However, the Taylor coefficients  $a_k$  are not optimal due to truncation, and a more accurate evaluation is desirable.

One can, instead, find the optimal  $\mathcal{L}^2$  approximation to  $f(\mathbf{A})\mathbf{x}$  within the  $m$ -dimensional *Krylov subspace*  $\mathcal{K}_m$  (with  $m \ll 3N$ ) generated by  $\mathbf{A}$  and  $\mathbf{x}$ :

$$\mathcal{K}_m(\mathbf{A}, \mathbf{x}) := \text{span}(\mathbf{x}, \mathbf{A}\mathbf{x}, \dots, \mathbf{A}^{m-1}\mathbf{x}).$$

Note that, as exploited in the power method, the term  $\mathbf{A}^{m-1}\mathbf{x}$  approximates the dominant eigenvector, and thus, the Krylov subspace is an approximation of the subspace formed by the eigenvectors corresponding to the  $m$  largest eigenvalues [28]. An orthonormal basis  $\mathbf{X}_m$  for the Krylov subspace  $\mathcal{K}_m$  is efficiently found via *Arnoldi iteration* [3], which uses a stabilized Gram-Schmidt process [34] to compute  $\mathbf{X}_m := (\mathbf{x}_0, \dots, \mathbf{x}_{m-1}) \in \mathbb{C}^{3N \times m}$  as well as  $\mathbf{H}_m :=$

$\mathbf{X}_m^* \mathbf{A} \mathbf{X}_m \in \mathbb{C}^{m \times m}$ . The matrix  $\mathbf{H}_m$  is in upper Hessenberg form, and describes the projection of  $\mathbf{A}$  onto  $\mathcal{K}_m(\mathbf{A}, \mathbf{x})$  relative to the basis  $\mathbf{X}_m$ . Moreover, this Hessenberg matrix satisfies  $\mathbf{g}(\mathbf{A})\mathbf{x} = \mathbf{X}_m^* \mathbf{g}(\mathbf{H}_m) \mathbf{e}_1$  where  $\mathbf{e}_1 = (1, 0, \dots, 0)^t$  for any polynomial  $\mathbf{g}$  of order less than  $m$  (see [33], Lemma 3.1). One thus obtains the approximation

$$f(\mathbf{A})\mathbf{x} \approx \mathbf{X}_m^* f(\mathbf{H}_m) \mathbf{e}_1$$

where the initial problem of the evaluation of a function with  $3N \times 3N$  range has been reduced to the evaluation of a function with  $m \times m$  range, where  $m \ll 3N$  is the length of the Krylov basis.

*Final Evaluation.* Finally, the remaining function of a low-dimensional matrix can be efficiently evaluated by  $f(\mathbf{H}_m) = \mathcal{T}^\top f(\mathcal{D}) \mathcal{T}$  via an unitary eigendecomposition of  $\mathbf{H}_m = \mathcal{T}^\top \mathcal{D} \mathcal{T}$ . Since  $\mathcal{D}$  is diagonal, the evaluation of  $f(\mathcal{D})$  can be done trivially, per diagonal element, with only  $m$  evaluations.

*Efficient Determination of Krylov Dimension.* To determine a conservative value of  $m$  such as the Krylov-based evaluations of matrix functions remain below a given error threshold, we follow [22]: the absolute error

$$\epsilon_m := \|f(\mathbf{A})\mathbf{x} - \mathbf{X}_m^* f(\mathbf{H}_m) \mathbf{e}_1\|$$

can be bounded from above by  $\epsilon_m \leq 10e^{-m^2/(5\rho)}$  if  $\sqrt{4\rho} \leq m \leq 2\rho$  and by  $\epsilon_m \leq 10/\rho e^{-\rho} \left(\frac{\rho}{m}\right)^m$  if  $m \geq 2\rho$  for  $f(\cdot) = \exp(\cdot)$  if the spectrum of the symmetric positive-definite system matrix  $\mathbf{A}$  is a subset of  $[0, 4\rho]$ . (Note that we approximate  $\rho$  with the use of a linear time Gershgorin circle approach, cf. Appendix B). Since other functions  $f$  can trivially be derived from matrix exponentials with trivial algebraic operations, it allows us to determine the basis length  $m$  for a given maximum desirable error.

## 4. Numerical Examples

All simulations that are shown in this section have been carried out on an Intel Core i7-3820QM processor with 16 GiB of memory.

<sup>1</sup>An excellent survey of suitable methods for the particular purpose of matrix exponential computation was published by [29]. Twenty-five years later, the same authors presented a revised version of their survey, cf. [30]. An enormous improvement has been achieved through the development of Krylov-type methods.

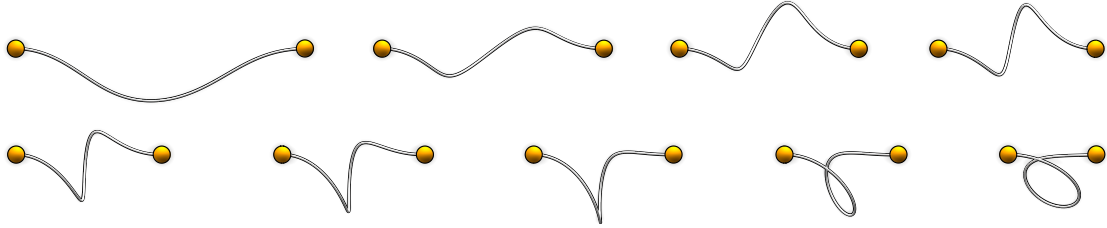


Figure 2: Canonical example from rod mechanics: demonstration of the buckling effect using the cuboidal fiber model and the DETI.

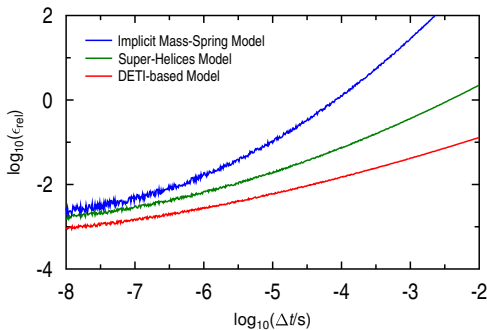


Figure 3: Illustration of the relative error  $\epsilon_{err}$  in dependency of the step size  $\Delta t$  for the implicit mass-spring model according to [36], the super-helices model according to [9], and the presented DETI-based method.

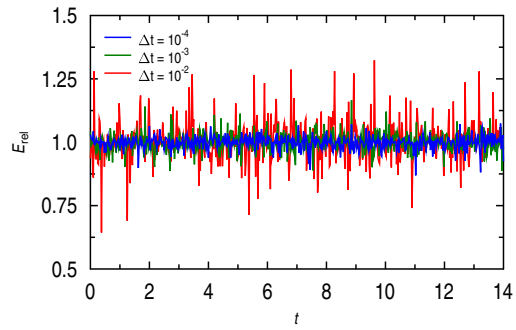


Figure 4: Illustration of the change of the relative energy  $E_{rel}$  in the undamped buckling scenario over time for three different step sizes  $\Delta t$ . It can clearly be seen, that the amplitude of the oscillating discrete energy does not increase over time which illustrates the symplectic behavior of the presented method in the undamped case.

#### 4.1. Validation of the Single Fiber Model

In this section we validate the numerical fiber model with respect to reliability, robustness, accuracy, and numerical stability.

*Buckling Effect.* In order to validate the reliability and robustness of the fiber model we first reproduce one of the canonical examples in rod mechanics—the buckling effect—by moving both ends of a fiber towards each other while at the same time twisting one end at a constant rate. The result is depicted in Fig. 2 and gives us the confidence that the numerical single fiber model is robust enough to handle typical deformations that occur during the simulation of fiber assemblies.

*Comparison with Cosserat Equations.* In a more elaborate experiment we validate our model against

the Cosserat equations in order to quantify its accuracy. The Cosserat equations describe the dynamic equilibrium of a one-dimensional continuum subject to external forces in terms of a set of nonlinear and coupled second order differential equations, cf. [2]. The numerical solution is more involved and we use a finite difference scheme in order to discretize the governing differential equations. More precisely, we make use of the formulation described in Appendix C. The final equations are then discretized by replacing the spatial derivatives with central differences and the temporal differences with forward differences. For small time steps this scheme allows to compute accurate solutions of the Cosserat equations which we use for the comparison with our method. As in our

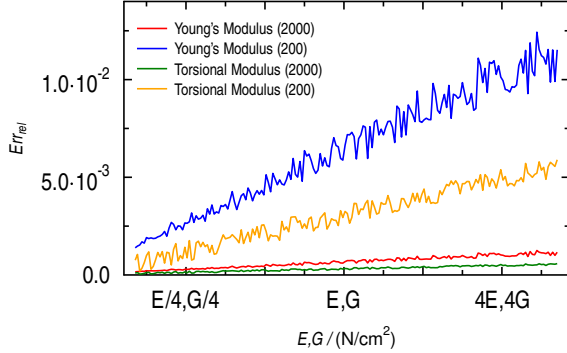


Figure 5: Comparison of our model with the results obtained by solving the Cosserat equations. The reference configuration is a single fiber with a helical shape that is fixed at one end and relaxes under the sole influence of gravity. The relative error  $Err_{rel}$  is shown for simultaneously varying Young’s modulus  $E$  and shear modulus  $G$  using two different discretizations with 2000 and 200 cuboids.

method, we make use of linear Rayleigh damping. The error is quantified by considering a helix relaxing under the influence of gravity and measuring the  $\mathcal{L}^2$ -norm of its maximum displacement obtained with our and with the Cosserat model after five oscillations. This measurement has repeatedly been carried out for varying values of the Young’s and the shear modulus, ranging from  $E/4$  to  $4E$  and  $G/4$  to  $4G$ , respectively. The respective base values have been set to  $E = 3.58 \cdot 10^5 \text{ Ncm}^{-2}$  and  $G = 1.07 \cdot 10^5 \text{ Ncm}^{-2}$ , which are typical parameters of human hair. The length of the fiber was  $L = 25.00 \text{ cm}$ , discretized with 2000 and 200 cuboids, the linear density was  $\lambda = 31.30 \mu\text{gcm}^{-1}$ , and the diameter  $d = 0.06 \text{ mm}$ . The results can be seen in Fig. 5. It shows that the error scales with the stiffness of the fiber. Increasing the number of cuboids by one order of magnitude causes an increase in accuracy by almost two orders in the case of Young’s modulus and only one order of magnitude in case of the shear modulus. Fig. 7 shows a sequence of rendered frames of the simulation.

*Comparison with other Rod / Fiber Models.* We also compared our approach against two other methods for the simulation of rods or fibers: a) the mass-spring model for hair simulation introduced in [36] and b)

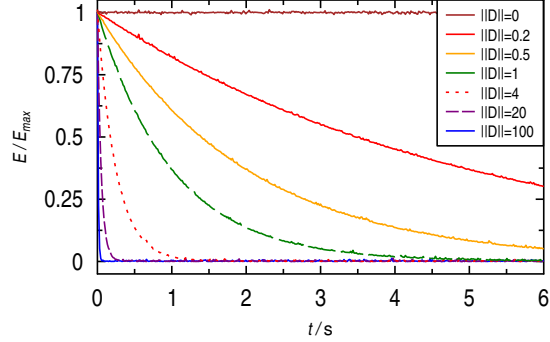


Figure 6: Illustration of the energy loss for different 2-norms of the damping matrix. For  $\|\mathbf{D}\| = 100$  there is an almost instant loss of the total energy of the system without any stability issues. For  $\|\mathbf{D}\| = 0$  the energy remains constant since our integration scheme is symplectic.

the so-called “super-helix” model from [9]. In particular, for the buckling rod example from Fig. 2 the evolution of the relative  $\mathcal{L}^2$ -error has been measured for varying step sizes. The results are shown in Fig. 3 and indicate that especially for “practical” step sizes of  $10^{-3}$  or larger the error of model b) is at least one order of magnitude larger than that produced by the DETI. The error of model a) is already out of bounds. From a point of view of computation time, the simulation of the buckling rod example from Fig. 2 takes about 0.6 s using our approach compared to about 8 s using the “super-helix” model, and 2.3 s using the mass-spring model from [36].

*Energy Preservation and Impact of Discretization.* Fig. 4 shows for varying step sizes that the energy of the buckling rod is fully preserved since the integration method is symplectic in the undamped case. While we always use a single layer discretization of the cross section the number of cuboids in longitudinal direction may vary from simulation to simulation. The impact of the longitudinal discretization (2000 and 200 segments) on the error is depicted in Fig. 5. The error scales linearly with the number of cuboids in longitudinal direction and quadratically with the number of cuboids per cross section (the latter is not shown in the diagram).

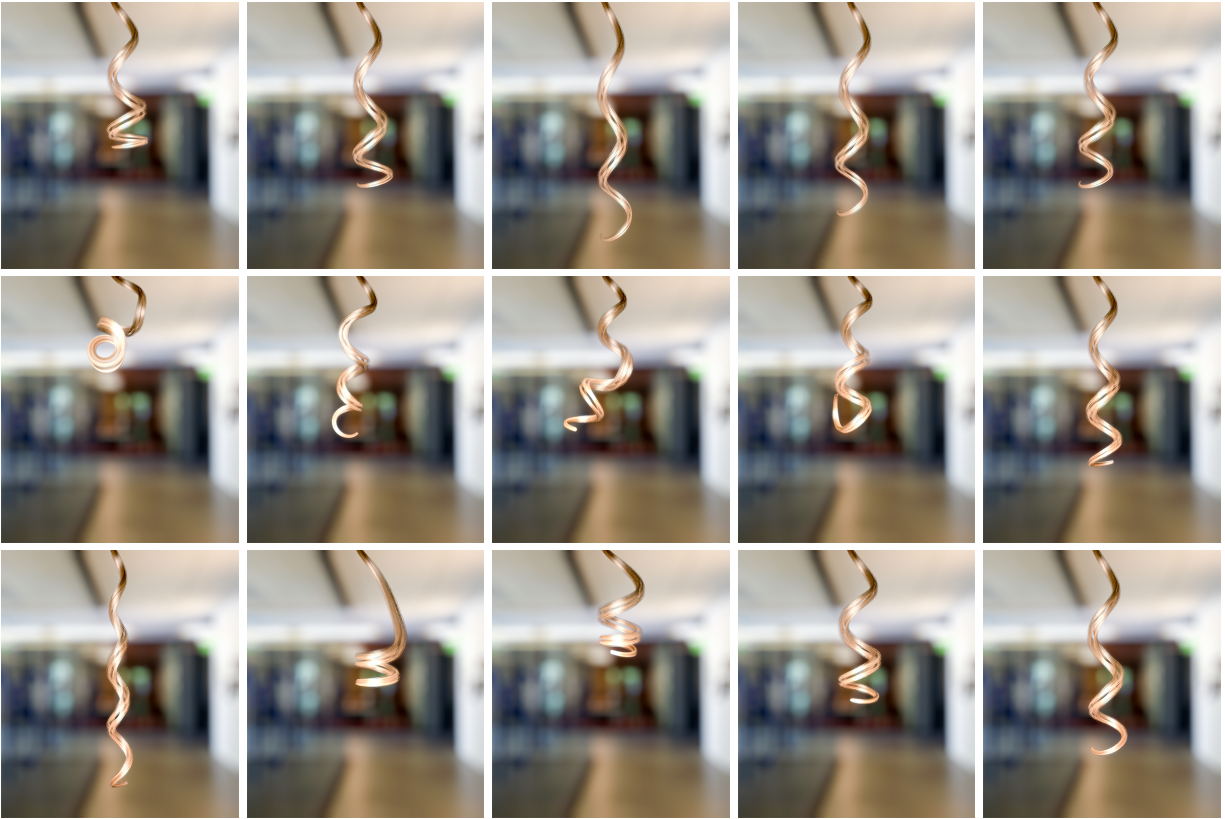


Figure 7: Simulation of a time varying elasticity (second row) and shear modulus (bottom row). The upper row shows the reference sequence of the strand relaxing under the influence of gravity. We only simulated the center line of the model with a subsequent interpolation of the remaining fibers.

#### 4.2. Analytical Treatment of Damping

Additionally, we simulated the scenario of a helix falling under the influence of gravity from Fig. 7 (upper row) using different intensities of damping, i.e. diagonal damping matrices  $\mathbf{D} = \alpha_0 \mathbf{M}$  of different 2-norms. The analytical treatment of damping results in the expected exponential decrease of energy. This decrease over time is illustrated in Fig. 6. For  $\|\mathbf{D}\| = 100$  there is an almost instant loss of the total energy of the system without any stability issues. Moreover, in the undamped case of  $\mathbf{D} = \mathbf{0}$ , the integrator is symplectic. This can be derived from the more general symplecticity statement proved in [26] since the total solution is constructed as a combination of a closed-form solution and a sinc<sup>2</sup>-filtered non-linearity with additional sinc-filter in its argument. Symplecticity directly implies that linear and angular momenta are accurately preserved. Furthermore, the energy is preserved in a way, that the amplitudes of the discrete energy oscillations are not increasing over time, cf. case  $\|\mathbf{D}\| = 0$  in Fig. 6.

*Summary.* It appears reasonable at this point to give the reader a concise summary of the beneficial qualities that characterize our approach:

- Analytical treatment of stiffness—allowing one to use larger time steps in very stiff scenarios when compared to other common approaches for fiber simulation.
- Analytical treatment of damping in the linear case—preventing numerical artifacts even for strong damping posing a real challenge to almost all commonly known fiber models, while implicit models induce uncontrollable artificial viscosity.
- Strict energy preservation caused by the symplectic nature of the DETI in the undamped case.
- Highly accurate numerical solutions comparable to that obtained with the classical Cosserat rod model discretized by a finite difference scheme.
- Accurate simulation of bending and twisting mode that enable the model to replicate the classical buckling effect known from rod mechanics.

- Mapping of real mechanical parameters to spring constants through a carefully chosen mesh topology: the Young’s and the shear modulus can be directly applied to the underlying oscillator network.

We conclude that the model presented herein offers high accuracy, speed (see Sec. 4.3), and robustness and at the same time the versatility of the prevalent oscillator networks.

#### 4.3. Fiber Assemblies and Fiber Meshes

The single fiber model can be easily extended for the simulation of fiber assemblies and fiber meshes.

*Fiber Assemblies.* In this example we simulated a hair ball consisting of over 25 000 single elements that was subject to abruptly accelerating and decelerating movements, cf. Fig. 8. The collisions that necessarily occurred between the fibers of the assembly among themselves and with the underlying ball geometry have been detected with a bounding volume hierarchy of axis-aligned bounding boxes. The system responded to the collisions by computing correction impulses of appropriate magnitudes, cf. [11]. Frictional effects have not been taken into account. Using a discretization of 50 cuboidal elements per fiber the whole simulation takes about 6 min for the DETI. In contrast, the particle-system approach of [36] needs 52 min, while using the “super-helix” model [9], the simulation requires 2 h and 17 min.

*Fiber Meshes.* Fiber meshes are composed of single fibers that are connected at the crossings by stiff springs. Fig. 9 and Fig. 10 show the simulation of a woven fabric made up of 2 500 individual fibers that was draped over an idol using our model. While in the first scene the damping was  $\|\mathbf{D}\| = 10$  it was increased to  $\|\mathbf{D}\| = 85$  in the second scene so that the cloth came to a rest very quickly. Due to our purely analytic approach to damping no stability issues or artifacts were observable. The collisions between the particles of the fabric have been resolved with the method explained above (but friction was enabled) while we used a force field based approach for the impacts between the fabric and the idol.



Figure 8: Simulation of a hair ball consisting of over 25 000 single elements. The collisions have been resolved by using correction impulses.

## 5. Conclusion

We have presented a novel numerical approach to the challenging topic of physically accurate and fast simulation of stiff fibers like human hair and fiber meshes. The cuboidal topology used in this model allows us to map real mechanical parameters like the Young’s and the shear modulus to the underlying oscillator networks. In a certain sense this opens up a path to deal with the influence of environmental conditions like air moisture and temperature when the functional dependencies of the mechanical parameters on these quantities are only practically determinable through a measurement in the laboratory. Beside this the fiber model is also surprisingly accurate as the thorough comparison against the Cosserat equations revealed. Bending, twisting, and buckling effects are reproduced with high reliability.

The bending and shearing stiffnesses of naturally occurring fibers differ by orders of magnitude because the underlying physical processes evolve on different time scales: the system is said to behave stiff. We have shown how one can effectively overcome this general and well-known problem of stable numerical integration of stiff differential equations: the application of a *Damped Exponential Time Integrator* (DETI) is a new and promising way in this regard. The effectiveness of the DETI lies in the analytical treatment of the stiff parts of the governing equations. The process of matrix function evaluation during time integration is accelerated by orders of magnitude using projection on lower dimensional Krylov subspaces. In addition, the purely analytical treatment of the damping part of the governing equations allows for a subtle control over the damping behavior

of the system without the bias caused by the intermixing of artificial viscosity induced by other commonly used numerical solution schemes.

One of the major shortcomings of the current approach is its inability to deal effectively with non-linear material behavior. Especially for the non-linearly damped case there is no known analytic solution, which in turn makes a numerical treatment of this part necessary—with all the known problems like uncontrollable energy loss through undesirable numerical viscosity. Another obvious drawback is that from a mathematical point of view it is not clear how the DETI integrates with non-smooth contact handling, since a lot of filtering is involved in stabilizing the solution. If, on the other hand, the old fashioned style of responding to collisions by applying arbitrarily stiff forces has been used previously and is viable for applications then the DETI is the first choice since even severely stiff collision response forces have no destabilizing impact on the solution process.

In our future work we aim to incorporate an effective treatment of non-linear and viscoelastic materials as naturally occurring fibers usually do not show a purely elastic material behavior.

## Acknowledgements

We are grateful to the financial support of the Max Planck Center for Visual Computing and Communication, the Federal Ministry of Education and Research of the Federal Republic of Germany, and the German National Merit Foundation. Moreover, our thanks go to the anonymous reviewers for many critical comments and feedback.

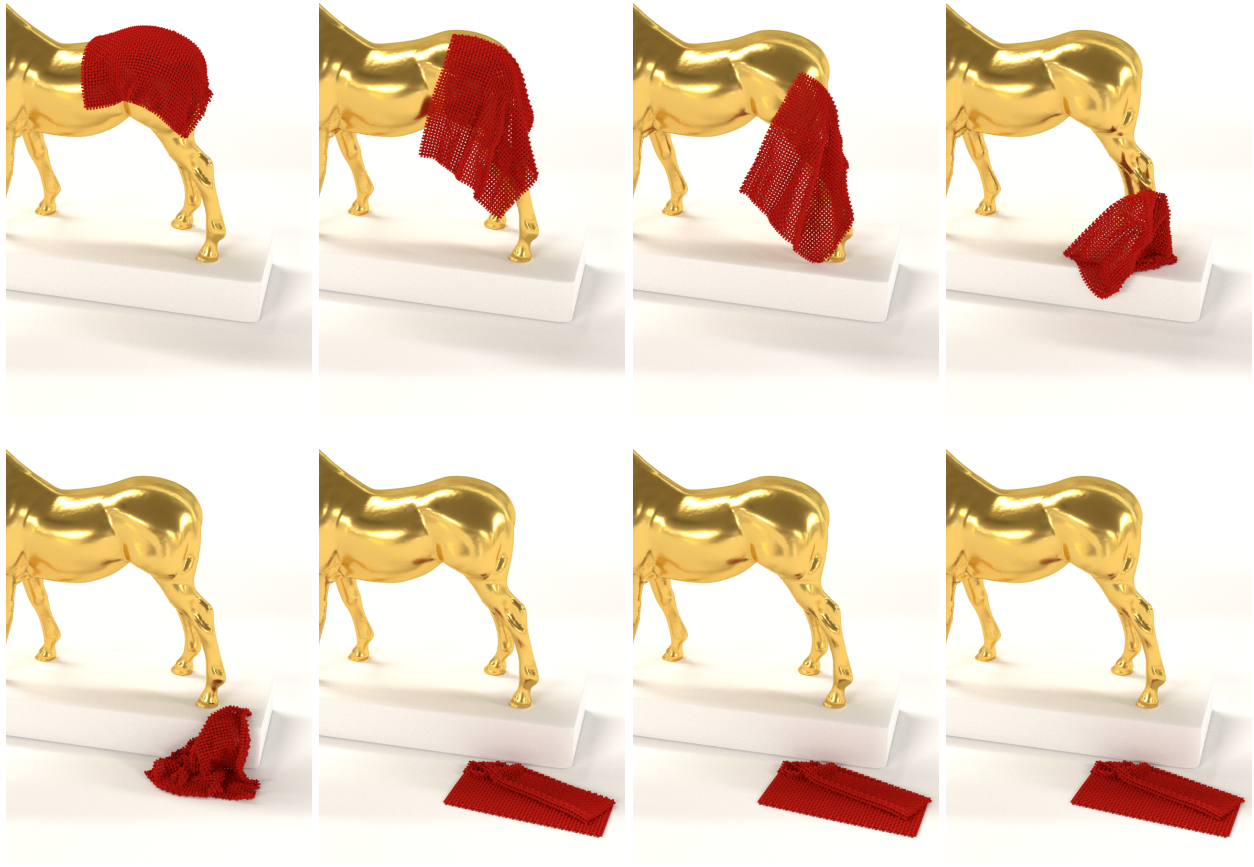


Figure 9: Simulation of a woven fabric made up of 2500 individual fibers using our model. The fibers are connected at the crossings by using very stiff springs. The collisions between the particles of the fabric have been resolved using correction impulses while we used a force-field-based approach for the impacts between the fabric and the idol. The damping was rather low ( $\|D\| = 10$ ).

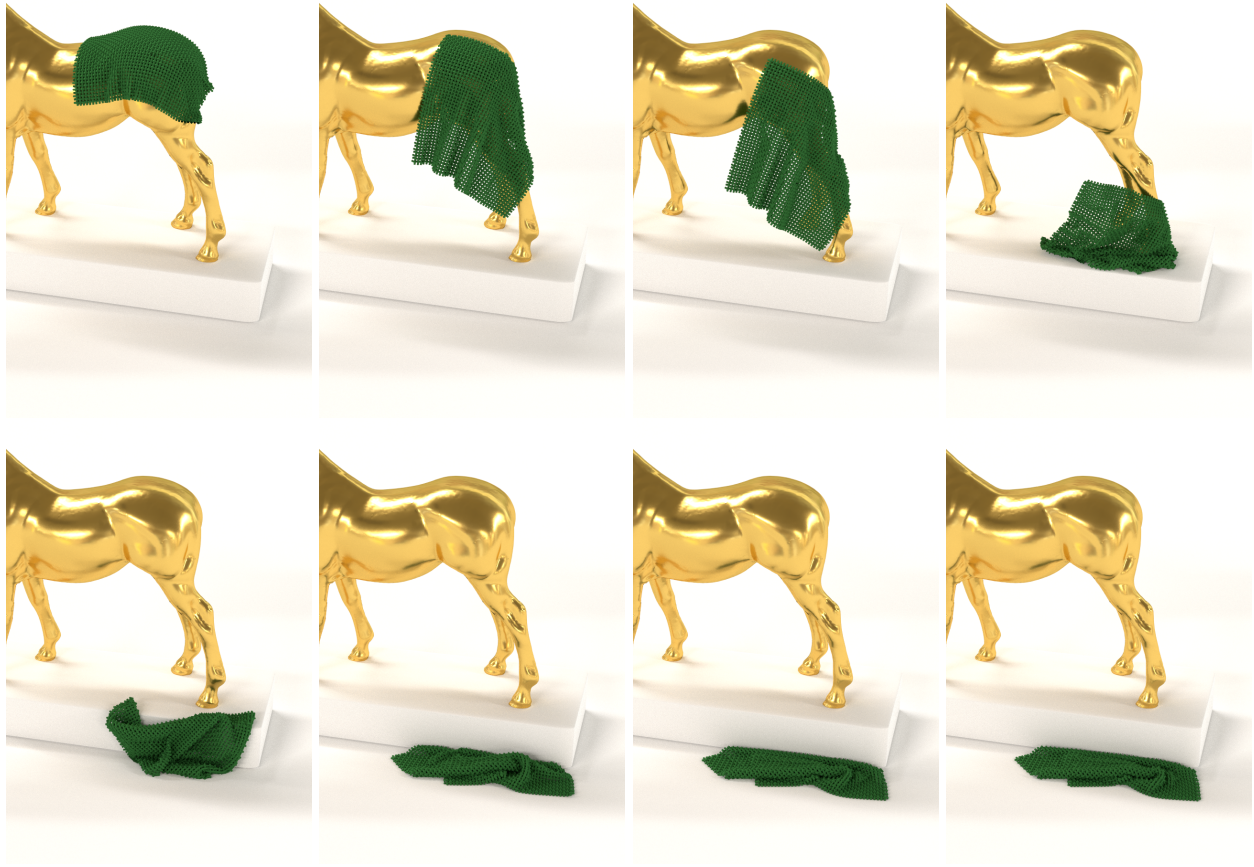


Figure 10: Simulation of a woven fabric made up of 2 500 individual fibers using our model. The fibers are connected at the crossings by using very stiff springs. The collisions between the particles of the fabric have been resolved using correction impulses while we used a force-field-based approach for the impacts between the fabric and the idol. In this example the damping was set to  $\|D\| = 85$  so that the cloth came to a rest very quickly. Due to our purely analytic approach to damping no stability issues or artifacts were observable.

## References

- [1] Anjyo, K.i., Usami, Y., Kurihara, T.: A simple method for extracting the natural beauty of hair. *ACM SIGGRAPH Comput. Graph.* **26**(2), 111–120 (1992)
- [2] Antman, S.S.: *Nonlinear Problems of Elasticity*, *Appl. Math. Sci.*, vol. 107. Springer-Verlag, Berlin and New York (1995)
- [3] Arnoldi, W.E.: The Principle of Minimized Iterations in the Solution of the Matrix Eigenvalue Problem. *Quarterly of Applied Mathematics* **9**, 17–29 (1951)
- [4] Baudet, V., Beuve, M., Jaillet, F., Shariat, B., Zara, F.: Integrating Tensile Parameters in Hexahedral Mass-Spring System for Simulation. In: *International Conference on Computer Graphics, Visualization and Computer Vision'2009 - WSCG'2009* (2009)
- [5] Baudet, V., Beuve, M., Jaillet, F., Shariat, B., Zara, F.: Integrating Tensile Parameters in Mass-Spring System for Deformable Object Simulation. Tech. Rep. RR-LIRIS-2009-034, LIRIS UMR 5205 CNRS/INSA de Lyon/Universit Claude Bernard Lyon 1/Universit Lumire Lyon 2/cole Centrale de Lyon (2009)
- [6] Bergou, M., Audoly, B., Vouga, E., Wardetzky, M., Grinspun, E.: Discrete viscous threads. *ACM Trans. Graph.* **29**(4), 116:1–116:10 (2010). DOI 10.1145/1778765.1778853. URL <http://doi.acm.org/10.1145/1778765.1778853>
- [7] Bergou, M., Wardetzky, M., Robinson, S., Audoly, B., Grinspun, E.: Discrete elastic rods. *ACM Trans. Graph.* **27**(3), 63:1–63:12 (2008)
- [8] Bertails, F.: Linear time super-helices. *Comput. Graph. Forum* **28**(2), 417–426 (2009)
- [9] Bertails, F., Audoly, B., Cani, M.P., Querleux, B., Leroy, F., Lévêque, J.L.: Super-helices for predicting the dynamics of natural hair. In: *ACM SIGGRAPH 2006 Papers, SIGGRAPH '06*, pp. 1180–1187. ACM, New York, NY, USA (2006)
- [10] Bianchi, G., Solenthaler, B., Székely, G., Harders, M.: Simultaneous topology and stiffness identification for mass-spring models based on fem reference deformations. In: C. Barillot (ed.) *Medical Image Computing and Computer-Assisted Intervention MICCAI 2004*, vol. 2, pp. 293–301. Springer (2004)
- [11] Bridson, R., Fedkiw, R., Anderson, J.: Robust treatment of collisions, contact and friction for cloth animation. In: *Proceedings of the 29th annual conference on Computer graphics and interactive techniques, SIGGRAPH '02*, pp. 594–603. ACM, New York, NY, USA (2002)
- [12] Bridson, R., Marino, S., Fedkiw, R.: Simulation of clothing with folds and wrinkles. In: *Proceedings of the 2003 ACM SIGGRAPH/Eurographics symposium on Computer animation, SCA '03*, pp. 28–36. Eurographics Association, Aire-la-Ville, Switzerland, Switzerland (2003)
- [13] Cani, E.P.M.P., Plante, E., paule Cani, M., Poulin, P.: Capturing the complexity of hair motion. *Graphical Models* **64**, 40–58 (2002)
- [14] Choe, B., Choi, M.G., Ko, H.S.: Simulating complex hair with robust collision handling. In: *Proceedings of the 2005 ACM SIGGRAPH/Eurographics symposium on Computer animation, SCA '05*, pp. 153–160. ACM, New York, NY, USA (2005)
- [15] Choi, K.J., Ko, H.S.: Stable but responsive cloth. In: *Proceedings of the 29th annual conference on Computer graphics and interactive techniques, SIGGRAPH '02*, pp. 604–611. ACM, New York, NY, USA (2002)
- [16] Eitzmuß, O., Keckeisen, M., Straßer, W.: A fast finite element solution for cloth modelling. In: *Proceedings of the 11th Pacific Conference on Computer Graphics and Applications, PG '03*, pp. 244–. IEEE Computer Society, Washington, DC, USA (2003)
- [17] Featherstone, R.: *Robot Dynamics Algorithms*. Kluwer Academic Publishers (1987)

- [18] Gerschgorin, S.A.: Über die Abgrenzung der Eigenwerte einer Matrix. Bulletin de l'Académie des Sciences de l'URSS. Classe des sciences mathématiques et na **6**, 749–754 (1931)
- [19] Gusev, A.A.: Finite element mapping for spring network representations of the mechanics of solids. Phys. Rev. Lett. **93**, 034,302 (2004)
- [20] Hadap, S.: Oriented strands: dynamics of stiff multi-body system. In: Proceedings of the 2006 ACM SIGGRAPH/Eurographics symposium on Computer animation, SCA '06, pp. 91–100. Eurographics Association, Aire-la-Ville, Switzerland, Switzerland (2006)
- [21] Hadap, S., Magnenat-Thalmann, N.: Modeling dynamic hair as a continuum. Computer Graphics Forum **20**(e 3), 329–338 (2001)
- [22] Hochbruck, M., Lubich, C.: On Krylov subspace approximations to the matrix exponential operator. SIAM Journal on Numerical Analysis **34**(5), 1911–1925 (1997)
- [23] Kirchhoff, G.R.: Über das Gleichgewicht und die Bewegung eines unendlich dünnen elastischen Stabes. Journal für die Reine und angewandte Mathematik **56**, 285–313 (1859)
- [24] Liu, M., Gorman, D.: Formulation of Rayleigh damping and its extensions. Computers & Structures **57**(2), 277 – 285 (1995)
- [25] Lloyd, B.A., Kirac, S., Székely, G., Harders, M.: Identification of Dynamic Mass Spring Parameters for Deformable Body Simulation. In: Eurographics 2008 - Short Papers, pp. 131–134 (2008)
- [26] Michels, D.L., Sobottka, G.A., Weber, A.G.: Exponential integrators for stiff elastodynamic problems. ACM Trans. Graph. **33**(1), 7:1–7:20 (2014)
- [27] Mirtich, B.V.: Impulse-based dynamic simulation of rigid body systems. Ph.D. thesis (1996). AAI9723116
- [28] Mises, R., Pollaczek-Geiringer, H.: Praktische Verfahren der Gleichungsauflösung. Zeitschrift für Angewandte Mathematik und Mechanik **9**, 152–164 (1929)
- [29] Moler, C., Loan, C.V.: Nineteen Dubious Ways to Compute the Exponential of a Matrix. SIAM Review **20**(4), 801–836 (1978)
- [30] Moler, C., Loan, C.V.: Nineteen dubious ways to compute the exponential of a matrix, twenty-five years later. SIAM Review **45**(1), 3–49 (2003)
- [31] Pai, D.K.: STRANDS: interactive simulation of thin solids using cosserat models. Comput. Graph. Forum **21**(3), 347–352 (2002)
- [32] Rosenblum, R.E., Carlson, W.E., Tripp, E.: Simulating the structure and dynamics of human hair: modeling, rendering and animation. The Journal of Visualization and Computer Animation **2**(4) (1991)
- [33] Saad, Y.: Analysis of some Krylov subspace approximations to the matrix exponential operator. SIAM Journal on Numerical Analysis **29**, 209–228 (1992)
- [34] Saad, Y.: Iterative Methods for Sparse Linear Systems, 2 edn. SIAM (2003)
- [35] San-Vicente, G., Aguinaga, I., Celigueta, J.T.: Cubical mass-spring model design based on a tensile deformation test and nonlinear material model. IEEE Transactions on Visualization and Computer Graphics **18**(2), 228–241 (2012)
- [36] Selle, A., Lentine, M., Fedkiw, R.: A mass spring model for hair simulation. ACM Trans. Graph. **27**(3), 64:1–64:11 (2008)
- [37] Sobottka, G., Lay, T., Weber, A.: Stable integration of the dynamic cosserat equations with application to hair modeling. Journal of WSCG **16**(1-3), 73–80 (2008)
- [38] Spillmann, J., Teschner, M.: Corde: Cosserat rod elements for the dynamic simulation of one-dimensional elastic objects. In: Proceedings of

the 2007 ACM SIGGRAPH/Eurographics symposium on Computer animation, SCA '07, pp. 63–72. Eurographics Association, Aire-la-Ville, Switzerland, Switzerland (2007)

- [39] Teschner, M., Heidelberger, B., Muller, M., Gross, M.: A versatile and robust model for geometrically complex deformable solids. In: Proceedings of the Computer Graphics International, CGI '04, pp. 312–319. IEEE Computer Society, Washington, DC, USA (2004)
- [40] Umetani, N., Schmidt, R., Stam, J.: Position-based elastic rods. In: ACM SIGGRAPH 2014 Talks, SIGGRAPH '14, pp. 47:1–47:1. ACM, New York, NY, USA (2014). DOI 10.1145/2614106.2614158. URL <http://doi.acm.org/10.1145/2614106.2614158>
- [41] Van Gelder, A.: Approximate simulation of elastic membranes by triangulated spring meshes. *J. Graph. Tools* **3**(2), 21–42 (1998)

## Appendix A. Nonlinear Materials and Mechanical Parameter Mapping

In order to derive analytical expressions for the mapping of the mechanical parameters to the spring stiffnesses of a cuboid one first has to consider the potential energy for the unit elongation and unit shearing of a cuboid, derive the equations of motions for the system, and solve for the stiffness constants. Similar to the approach presented in [4], we have derived analytical expressions to set up the stiffnesses of our fiber system.

Let us consider a fiber of length  $\ell$  approximated with  $N := 4 \cdot (N_C + 1)$  particles arranged on  $N_C$  cuboids with side lengths  $\ell_1, \ell_2, \ell_3$ , where  $\ell_1$  denotes the length of the edges parallel to the midline and  $\ell_2, \ell_3$  are the lengths of the edges orthogonal to them. The respective mappings for the stiffnesses

of a cuboidal element are then given by

$$k_{t\ell_i} := \frac{G}{12\ell_1\ell_2\ell_3} \left( \frac{3E}{G} \prod_{j=1}^3 \ell_j^{2(1-\delta_{ij})} + (\ell_1^2 + \ell_2^2 + \ell_3^2) \cdot \left( \left( \frac{E}{2G} - 1 \right) \sum_{j=1}^3 (1 - \delta_{ij}) \ell_j^2 - \ell_i^2 \right) \right)$$

and

$$k_d := \frac{G}{12\ell_1\ell_2\ell_3} (\ell_1^2 + \ell_2^2 + \ell_3^2),$$

in which  $E$  denotes the Young's modulus and  $G$  denotes the shear modulus. The equilibrium length of each spring is equal to the Euclidean distance between the particles in the undeformed state of a cuboid. Note, that the tension springs do not have the same stiffnesses since they depend on the equilibrium lengths  $\ell_1, \ell_2, \ell_3$ . In addition we have to incorporate six correction forces ( $\mathbf{F}_{\ell_1\ell_2}, \mathbf{F}_{\ell_1\ell_3}, \mathbf{F}_{\ell_2\ell_1}, \mathbf{F}_{\ell_2\ell_3}, \mathbf{F}_{\ell_3\ell_1}, \mathbf{F}_{\ell_3\ell_2}$ ) handled as external forces, with norms

$$F_{\ell_j\ell_i} := -\frac{F_{\ell_i}}{48} \prod_{l=1}^3 \ell_l^{\delta_{il} + \delta_{jl} - 2} \left( 6 \left( \frac{E}{2G} - 1 \right) \prod_{l=1}^3 \ell_l^{2(1-\delta_{il})} + (\ell_1^2 + \ell_2^2 + \ell_3^2) \left( \left( \frac{E}{2G} - 1 \right) \sum_{l=1}^3 (1 - \delta_{jl}) \ell_l^2 - \ell_i^2 \right) \right)$$

acting along  $\ell_j$  for the elongation along  $\ell_i$  induced by the linear internal spring force  $F_{\ell_i}$ .

In addition, we assume a homogeneous mass distribution so that each particle mass is given by  $m := \rho \ell / N$  in the case of a linear material density  $\rho$  per unit length. We set  $\ell_1 := \ell / N_C$ ,  $\ell_2 := \ell_3 := \sqrt{\pi} / 2d$  where  $d$  is the diameter of the fiber to preserve the volume of an enclosed cylindrical segment.

## Appendix B. Estimation of the Eigenvalues

For a matrix  $\mathbf{A} \in \mathbb{C}^{3N \times 3N}$ , the Gershgorin circles  $\mathbf{G}_1, \dots, \mathbf{G}_{3N}$  are defined by  $\mathbf{G}_i := \mathcal{S}(a_{ii}, \sum_{j=1..3N} |a_{ij}|)$  for  $i \in \{1, \dots, 3N\}$ . We denote by  $\mathcal{S}(x, r)$  the circle of center  $x \in \mathbb{C} \cong \mathbb{R}^2$  with radius  $r \in \mathbb{R}$ . According to Gershgorin's circle theorem, the spectrum of  $\mathbf{A}$  is a subset of the union of all

Gershgorin circles  $\mathbf{G}^\circ := \bigcup_{i=1}^{3N} \mathbf{G}_i$ . Furthermore, the number of Gershgorin circles included in each connected component of  $\mathbf{G}^\circ$  are equal to the numbers of eigenvalues included in the same components, see [18]. This is used to easily determine approximations to the extremal eigenvalues of the matrix  $\mathbf{A}$ . If  $\mathbf{A}$  is symmetric, the spectrum of  $\mathbf{A}^\top$  is identical and a second estimation can be realized using columnwise evaluated Gershgorin circles. If  $\mathbf{A}$  is sparse, the whole process has linear complexity.

### Appendix C. Theory of Cosserat Rods

Fibers can approximately be considered as one-dimensional continua that undergo bending, twisting, shearing, and longitudinal dilation deformation. Modeling the twisting behavior correctly requires that we are able to measure the rotation around the local tangent of the centerline of a fiber. Local orientation fields are usually present in one-dimensional theories such that of the special Cosserat Theory of rods. Following [2], we consider the Euclidian 3-space  $\mathbb{E}^3$  to be the abstract 3-dimensional inner product space. Its elements are denoted by lower-case, boldface, italic symbols. Let  $\mathbb{R}^3$  be the set of triples of real numbers. Its elements are denoted by lower-case, boldface, sans-serif letters.

The motion of a special Cosserat Rod is given by

$$(s, t) \mapsto (\mathbf{r}(s, t), \mathbf{d}_1(s, t), \mathbf{d}_2(s, t)), \quad (\text{C.1})$$

where  $\mathbf{r}(s, t)$  is the centerline of the rod. It is furnished with a set of so-called orthonormal directors

$$\{\mathbf{d}_1(s, t), \mathbf{d}_2(s, t), \mathbf{d}_3(s, t)\}.$$

$\{\mathbf{d}_k\}$  is a right-handed orthonormal basis in  $\mathbb{E}^3$ , with  $\mathbf{d}_3 := \mathbf{d}_1 \times \mathbf{d}_2$ . The directors  $\mathbf{d}_1$  and  $\mathbf{d}_2$  span the cross-section plane, see Fig. C.11. The deformation of the rod is obtained if its motion defined by Eq. (C.1) is related to some reference configuration

$$\{\mathbf{r}^\circ(s, t), \mathbf{d}_1^\circ(s, t), \mathbf{d}_2^\circ(s, t)\}.$$

Further, there exist vector-valued functions  $\boldsymbol{\kappa}$  and  $\boldsymbol{\omega}$  such that the directors evolve according to the kinematic relations

$$\begin{aligned} \partial_s \mathbf{d}_k &= \boldsymbol{\kappa} \times \mathbf{d}_k, \\ \partial_t \mathbf{d}_k &= \boldsymbol{\omega} \times \mathbf{d}_k, \end{aligned}$$

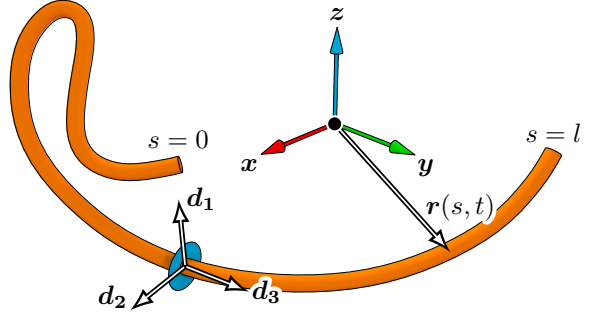


Figure C.11: The vector set  $\{\mathbf{d}_k\}$  forms an orthonormal right-handed trihedron at each point of the curve. Thereby  $\mathbf{d}_1$  and  $\mathbf{d}_2$  span the local material cross-section, whereas  $\mathbf{d}_3$  is perpendicular to the material cross section. Since shear deformations are included,  $\mathbf{d}_3$  is in general not equal to the local tangent to the curve.

where  $\boldsymbol{\kappa}$  is the Darboux and  $\boldsymbol{\omega}$  the twist vector. Their components are given with respect to the orthonormal basis, i.e.  $\boldsymbol{\kappa} = \sum_{k=1}^3 \kappa_k \mathbf{d}_k$  and  $\boldsymbol{\omega} = \sum_{k=1}^3 \omega_k \mathbf{d}_k$ . The linear strains of the rod are given by

$$\boldsymbol{\nu} = \sum_{k=1}^3 \nu_k \mathbf{d}_k = \partial_s \mathbf{r}$$

and the velocity of a cross-section material plane by  $\mathbf{v} = \partial_t \mathbf{r}$ . The triples  $(\kappa_1, \kappa_2, \kappa_3)$ ,  $(\omega_1, \omega_2, \omega_3)$ ,  $(\nu_1, \nu_2, \nu_3)$ , and  $(v_1, v_2, v_3)$  are denoted by  $\boldsymbol{\kappa}$ ,  $\boldsymbol{\omega}$ ,  $\boldsymbol{\nu}$ , and  $\mathbf{v}$  respectively. In particular,  $\boldsymbol{\kappa} := (\kappa_1, \kappa_2, \kappa_3)$  and  $\boldsymbol{\nu} := (\nu_1, \nu_2, \nu_3)$  are the strain variables that uniquely determine the motion of the rod described by Eq. (C.1) at every instant in time  $t$  (except for a rigid body motion). Their components have a physical meaning: they describe the bending of the rod with respect to the two major axes of the cross section  $(\kappa_1, \kappa_2)$ , the torsion  $(\kappa_3)$ , shear  $(\nu_1, \nu_2)$  and extension  $(\nu_3)$ . Moreover, since

$$\partial_t \partial_s \mathbf{d}_k = \partial_s \partial_t \mathbf{d}_k$$

we obtain the compatibility equation

$$\partial_t \boldsymbol{\kappa} = \partial_s \boldsymbol{\omega} - \boldsymbol{\omega} \times \boldsymbol{\kappa}.$$

In the same sense we have

$$\partial_t \boldsymbol{\nu} = \partial_s \mathbf{v}.$$

### Appendix C.1. Equations of Motion

The equations of motion for the rod read

$$\begin{aligned}\partial_s \mathbf{n} + \mathbf{f} &= \rho A \partial_t \mathbf{v} + \rho (I_1 \partial_{tt} \mathbf{d}_1 + I_2 \partial_{tt} \mathbf{d}_2), \\ \partial_s \mathbf{m} + \boldsymbol{\nu} \times \mathbf{n} + \mathbf{l} &= \rho (I_1 \mathbf{d}_1 + I_2 \mathbf{d}_2) \\ &\quad \times \partial_t \mathbf{v} + \partial_t (\rho \mathbf{J} \boldsymbol{\omega}),\end{aligned}$$

where  $\mathbf{n} = \sum_{k=1}^3 n_k \mathbf{d}_k$  and  $\mathbf{m} = \sum_{k=1}^3 m_k \mathbf{d}_k$  are the internal stresses and  $\mathbf{f}$  and  $\mathbf{l}$  are the external forces and torques acting on the rod,  $\rho$  the linear density.  $I_1$  and  $I_2$  are the first mass moments of inertia of cross section per unit length and  $\mathbf{J}$  is the inertia tensor of cross section per unit length. Further, we define  $\mathbf{n} := (n_1, n_2, n_3)$  and  $\mathbf{m} := (m_1, m_2, m_3)$ . The shear forces are given by  $n_1$  and  $n_2$ , the tension by  $\mathbf{n} \cdot \boldsymbol{\nu} / \|\boldsymbol{\nu}\|$ , bending moments by  $m_1$  and  $m_2$ , and the twisting moment by  $m_3$ .

### Appendix C.2. Constitutive Relations

In order to relate the internal stresses  $\mathbf{n}$  and  $\mathbf{m}$  to the kinematic quantities  $\boldsymbol{\nu}$  and  $\boldsymbol{\kappa}$  we introduce constitutive equations of the form

$$\begin{aligned}\mathbf{n}(s, t) &= \hat{\mathbf{n}}(\boldsymbol{\kappa}(s, t), \boldsymbol{\nu}(s, t), s), \\ \mathbf{m}(s, t) &= \hat{\mathbf{m}}(\boldsymbol{\kappa}(s, t), \boldsymbol{\nu}(s, t), s).\end{aligned}$$

For fixed  $s$ , the common domain  $\mathcal{V}(s)$  of these constitutive functions is a subset of  $(\boldsymbol{\kappa}, \boldsymbol{\nu})$  describing orientation preserving deformations.  $\mathcal{V}(s)$  consists at least of all  $(\boldsymbol{\kappa}, \boldsymbol{\nu})$  that satisfy

$$\nu_3 = \boldsymbol{\nu} \cdot \mathbf{d}_3 > 0.$$

The rod is called hyper-elastic, if there exists a strain-energy-function

$$W : \{(\boldsymbol{\kappa}, \boldsymbol{\nu} \in \mathcal{V})\} \rightarrow \mathbb{R}$$

such that

$$\begin{aligned}\hat{\mathbf{n}}(\boldsymbol{\kappa}, \boldsymbol{\nu}, s) &= \partial W(\boldsymbol{\kappa}, \boldsymbol{\nu}, s) / \partial \boldsymbol{\nu}, \\ \hat{\mathbf{m}}(\boldsymbol{\kappa}, \boldsymbol{\nu}, s) &= \partial W(\boldsymbol{\kappa}, \boldsymbol{\nu}, s) / \partial \boldsymbol{\kappa}.\end{aligned}$$

The rod is called viscoelastic of strain-rate type of complexity 1 if there exist functions such that

$$\begin{aligned}\mathbf{n}(s, t) &= \hat{\mathbf{n}}(\boldsymbol{\kappa}(s, t), \boldsymbol{\nu}(s, t), \partial_t \boldsymbol{\kappa}(s, t), \partial_t \boldsymbol{\nu}(s, t), s), \\ \mathbf{m}(s, t) &= \hat{\mathbf{m}}(\boldsymbol{\kappa}(s, t), \boldsymbol{\nu}(s, t), \partial_t \boldsymbol{\kappa}(s, t), \partial_t \boldsymbol{\nu}(s, t), s).\end{aligned}$$

For  $\partial_t \boldsymbol{\kappa}(s, t) = \mathbf{0}$  and  $\partial_t \boldsymbol{\nu}(s, t) = \mathbf{0}$ , these equations become the so called equilibrium response functions and describe elastic behavior.

### Appendix C.3. Material Laws

The constitutive laws for elastic material behavior become

$$\hat{\mathbf{n}}(s, t) = (GA(\nu_1 - \nu_1^\circ), GA(\nu_2 - \nu_2^\circ), EA(\nu_3 - \nu_3^\circ))$$

with the initial strain vector field  $\boldsymbol{\nu}^\circ(s)$ , Young's modulus  $E$ , cross-section area  $A$ , and

$$\begin{aligned}\hat{\mathbf{m}}(s, t) &= (E_b I_1 (\kappa_1 - \kappa_1^\circ), E_b I_2 (\kappa_2 - \kappa_2^\circ), \\ &\quad G I_3 (\kappa_3 - \kappa_3^\circ))\end{aligned}$$

with the initial bending and torsion vector field  $\boldsymbol{\kappa}^\circ(s)$ , Young's modulus  $E_b$  of bending, and shear modulus  $G$ . The area moments of inertia are again denoted by  $I_1$  and  $I_2$ , the polar moment of inertia with  $I_3$ .

#### Appendix C.3.1. Kirchhoff Rods

We allude to the fact that in the classical theory of Kirchhoff the rod can undergo neither shear nor extension. This is accommodated by setting the linear strains to

$$\boldsymbol{\nu} := (\nu_1, \nu_2, \nu_3) = (0, 0, 1)$$

in local coordinates. Geometrically this means, that the angle between the director  $\mathbf{d}_3$  and the tangent to the centerline,  $\partial_s \mathbf{r}$ , always remains zero (no shear) and that the tangent to the centerline always has unit length (no elongation).

### Appendix C.4. System of Governing Equations

The full system of partial differential equations governing the deformation of an elastic rod is thus given by the following first order system,

$$\begin{aligned}\partial_t \mathbf{d}_k &= \boldsymbol{\omega} \times \mathbf{d}_k, \\ \partial_t \boldsymbol{\kappa} &= \partial_s \boldsymbol{\omega} - \boldsymbol{\omega} \times \boldsymbol{\kappa}, \\ \partial_t \boldsymbol{\nu} &= \partial_s \mathbf{v}, \\ \partial_t (\rho \mathbf{J} \boldsymbol{\omega}) &= \partial_s (\hat{m}_k(\boldsymbol{\kappa}, \boldsymbol{\nu}) \mathbf{d}_k) + \boldsymbol{\nu} \times \hat{n}_k(\boldsymbol{\kappa}, \boldsymbol{\nu}) \mathbf{d}_k, \\ \rho A \partial_t \mathbf{v} &= \partial_s (\hat{n}_k(\boldsymbol{\kappa}, \boldsymbol{\nu}) \mathbf{d}_k).\end{aligned}\tag{C.2}$$

If  $(\hat{\mathbf{n}}, \hat{\mathbf{m}})$  satisfy the monotonicity condition, i.e. the matrix

$$\begin{bmatrix} \partial \hat{\mathbf{m}} / \partial \boldsymbol{\kappa} & \partial \hat{\mathbf{m}} / \partial \boldsymbol{\nu} \\ \partial \hat{\mathbf{n}} / \partial \boldsymbol{\kappa} & \partial \hat{\mathbf{n}} / \partial \boldsymbol{\nu} \end{bmatrix},$$

is positive-definite, then this system is hyperbolic. It can be written in the form of a conservation law

$$\partial_t \Phi(\zeta) = \partial_s \Psi(\zeta) + \Theta(\zeta),$$

with  $\zeta = (\mathbf{d}_k, \boldsymbol{\kappa}, \boldsymbol{\nu}, \boldsymbol{\omega}, \mathbf{v})$ . This system can be decoupled from the Kinematic Eq. (C.2) by decomposing it with respect to the basis  $\{\mathbf{d}_k\}$  which yields

$$\begin{aligned} \partial_t \boldsymbol{\kappa} &= \partial_s \boldsymbol{\omega} - \boldsymbol{\omega} \times \boldsymbol{\kappa}, \\ \partial_t \boldsymbol{\nu} &= \partial_s \mathbf{v} + \boldsymbol{\kappa} \times \mathbf{v} - \boldsymbol{\omega} \times \boldsymbol{\nu}, \\ \partial_t (\rho \mathbf{J} \boldsymbol{\omega}) &= \partial_s \hat{\mathbf{m}} + \boldsymbol{\kappa} \times \hat{\mathbf{m}} + \boldsymbol{\nu} \times \hat{\mathbf{n}} - \boldsymbol{\omega} \times (\rho \mathbf{J} \boldsymbol{\omega}), \\ \rho A \partial_t \mathbf{v} &= \partial_s \hat{\mathbf{n}} + \boldsymbol{\kappa} \times \hat{\mathbf{n}} - \boldsymbol{\omega} \times (\rho A \mathbf{v}). \end{aligned} \quad (\text{C.3})$$

If external forces (e.g. gravity) are to be considered as well, they have to be added to the right-hand side of Eq. (C.3) after transforming them into the local basis. For this purpose the Kinematic Eq. (C.2) has to be solved additionally.

#### *Mechanical Parameters*

The following parameters influence the dynamic behavior of the fiber the density  $\rho$ , the cross-section area  $A = \pi ab$ , the area moments of inertia  $I_1 = \pi/4ab^3$ ,  $I_2 = \pi/4a^3b$  of the elliptic fiber cross section with semi-major axis lengths  $a, b$ , and the polar moment of inertia  $I_3 = I_1 + I_2$ . The corresponding inertia tensor is approximately given by

$$\mathbf{J} \approx \rho \cdot \text{diag}(ab/4, ab/4, ab/2).$$

The constitutive laws for elastic material behavior become

$$\hat{\mathbf{n}}(s, t) = (GA(\nu_1 - \nu_1^\circ), GA(\nu_2 - \nu_2^\circ), EA(\nu_3 - \nu_3^\circ))$$

with the initial strain vector field  $\boldsymbol{\nu}^\circ(s)$ , shear modulus  $G$ , Young's modulus  $E$ , and

$$\begin{aligned} \hat{\mathbf{m}}(s, t) &= (E_b I_1 (\kappa_1 - \kappa_1^\circ), E_b I_2 (\kappa_2 - \kappa_2^\circ), \\ &\quad GI_3 (\kappa_3 - \kappa_3^\circ)), \end{aligned}$$

with the initial bending and torsion vector field  $\boldsymbol{\kappa}^\circ(s)$  and Young's modulus  $E_b$  of bending.